Intracranial Plaque Enhancement in Patients with Cerebrovascular Events on High-Spatial-Resolution MR Images[1]

Ye Qiao, PhD
Steven R. Zeiler, MD, PhD
Saeedeh Mirbagheri, MD
Richard Leigh, MD
Victor Urrutia, MD
Robert Wityk, MD
Bruce A. Wasserman, MD

Purpose: To characterize intracranial plaque inflammation in vivo by using three-dimensional (3D) high-spatial-resolution contrast material–enhanced black-blood (BB) magnetic resonance (MR) imaging and to investigate the relationship between intracranial plaque inflammation and cerebrovascular ischemic events.

Materials and Methods: The study was approved by the institutional review board and was HIPAA compliant. Twenty-seven patients (19 men; mean age, 56.8 years ± 12.4 [standard deviation]) with cerebrovascular ischemic events (acute stroke, n = 20; subacute stroke, n = 2; chronic stroke, n = 3; transient ischemic attack, n = 2) underwent 3D time-of-flight MR angiography and contrast-enhanced BB 3-T MR imaging for intracranial atherosclerotic disease. Each identified plaque was classified as either culprit (the only or most stenotic lesion upstream from a stroke), probably culprit (not the most stenotic lesion upstream from a stroke), or nonculprit (not within the vascular territory of a stroke). Plaque contrast enhancement was categorized on BB MR images (grade 0, enhancement less than or equal to that of normal arterial walls seen elsewhere; grade 1, enhancement greater than grade 0 but less than that of the pituitary infundibulum; grade 2, enhancement greater than or equal to that of the pituitary infundibulum), and degree of contrast enhancement was calculated. Associations of the likelihood of being a culprit lesion with both plaque contrast enhancement and plaque thickness were estimated with ordinal logistic regression.

Results: Seventy-eight plaques were identified in 20 patients with acute stroke (21 [27%] culprit, 12 [15%] probably culprit, and 45 [58%] nonculprit plaques). In these patients, grade 2 contrast enhancement was associated with culprit plaques (odds ratio 34.6; 95% confidence interval: 4.5, 266.5 compared with grade 0) when adjusted for plaque thickness. Grade 0 was observed in only nonculprit plaques. Culprit plaques had a higher degree of contrast enhancement than did nonculprit plaques (25.9% ± 13.4 vs 13.6% ± 12.3, P = .003).

Conclusion: Contrast enhancement of intracranial atherosclerotic plaque is associated with its likelihood to have caused a recent ischemic event and may serve as a marker of its stability, thereby providing important insight into stroke risk.

Online supplemental material is available for this article.

[1] From the Russell H. Morgan Department of Radiology and Radiological Sciences (Y.Q., S.M., B.A.W.) and Department of Neurology (S.R.Z., R.L., V.U., R.W.), Johns Hopkins Hospital, Johns Hopkins University School of Medicine, 367 East Park Building, 600 N Wolfe St, Baltimore, MD 21287. Received December 19, 2012; revision requested January 31, 2013; revision received June 24; accepted July 10; final version accepted October 8. **Address correspondence to** B.A.W. (e-mail: *bwasser@jhmi.edu*).

Intracranial atherosclerotic disease (ICAD) is a major cause of stroke worldwide and is responsible for 8%–10% of strokes in the United States (1,2). Histologic studies of postmortem specimens (3–5) have revealed a strong inflammatory response in patients with ICAD plaques thought to be culprit lesions (ie, those responsible for downstream ischemic events), reflecting increased macrophage infiltration and neovascularity (3); these studies also have revealed that the degree of inflammation might influence the likelihood of a stroke (6).

High-spatial-resolution contrast material–enhanced magnetic resonance (MR) imaging can be used to characterize the extracranial carotid wall in vivo and to identify features that indicate risk for disruption (7,8). One such feature is plaque inflammation, which can be detected by using gadolinium-containing contrast agents (8–11). The degree of enhancement is thought to reflect the level of inflammatory activity because of increased endothelial permeability and neovascularity, which is independently associated with recent cerebrovascular ischemic events (7). However, little is known about how inflammation detected with MR imaging in patients with intracranial plaques relates to stroke, largely because an MR imaging sequence capable of characterizing intracranial plaques in vivo did not exist previously (12,13). A three-dimensional (3D) MR imaging sequence that can be used to characterize intracranial plaque, including inflammatory features such as wall thickening and enhancement, was introduced relatively recently (12). The 3D feature is crucial to the accurate measurement of the inherently curved intracranial arteries (14), and it enables intracranial circulation to be captured as a volume acquisition so that a more global evaluation of multiple intracranial lesions can be achieved contemporaneously. Since ICAD tends to develop focally and affects multiple vessel segments (15), this provides an opportunity for a controlled comparison of the culprit lesion with the coexistent asymptomatic lesions given their development in the same genetic and environmental milieu.

The purpose of this study was to characterize intracranial plaque inflammation in vivo by using 3D high-spatial-resolution contrast-enhanced black-blood (BB) MR imaging and to investigate its relation to cerebrovascular ischemic events.

Advances in Knowledge

- On the basis of qualitative estimation, plaques thought to be responsible for downstream ischemic strokes (culprit lesions) had the strongest contrast enhancement compared with probably culprit and nonculprit plaques when adjusted for plaque thickness ($P = .004$), whereas nonculprit plaques were the only lesions that did not enhance.
- On the basis of quantitative measurements, culprit plaques had a higher degree of contrast enhancement than did nonculprit plaques (25.9% ± 13.4 vs 13.6% ± 12.3, $P = .003$).

Materials and Methods

The institutional review board approved this Health Insurance Portability and Accountability Act–compliant study and granted an exemption to allow inclusion of deidentified data of patients who did not provide written informed consent.

Implications for Patient Care

- Our findings suggest intracranial plaque enhancement at MR imaging can help identify lesions responsible for an ischemic event and can potentially serve as a marker of intracranial plaque instability and stroke risk.
- Three-dimensional contrast-enhanced high-spatial-resolution black-blood MR imaging has great potential as a diagnostic tool in the identification of intracranial plaque vulnerability and in the assessment of the effectiveness of new therapies.

Study Population

From September 2009 to August 2012, 50 patients from the Johns Hopkins Stroke Center were prospectively included. These patients had *(a)* intracranial stenosis of at least 50% in a large intracranial artery (eg, intracranial internal carotid artery, middle cerebral artery, anterior cerebral artery, posterior cerebral artery, vertebral artery, or basilar artery) based on the findings of preceding computed tomographic (CT) angiography, MR angiography, and/or catheter angiography (16) and *(b)* a transient ischemic attack or stroke in the distribution of the narrowed vessel. Exclusion criteria consisted of *(a)* contraindications to gadolinium-containing contrast agents ($n = 0$), *(b)* extracranial cervical artery stenosis of more than 50% (16) ipsilateral to the narrowed intracranial vessel ($n = 2$), *(c)* evidence of nonatherosclerotic intracranial vascular disease (vasculitis, $n = 8$; Moya-Moya disease, $n = 1$; dissection, $n = 4$; reversible cerebral vasoconstriction syndrome, $n = 1$; and idiopathic stenosis with no more than one cardiovascular risk factor, $n = 5$), *(d)* evidence of cardiac sources of emboli ($n = 0$), and *(e)* MR images that were uninterpretable because of patient motion ($n = 2$). This left 27 patients for analysis. Patients were

Published online before print
10.1148/radiol.13122812 **Content codes:** NR MR

Radiology 2014; 271:534–542

Abbreviations:
BB = black blood
CI = confidence interval
ICAD = intracranial atherosclerotic disease
3D = three-dimensional
TOF = time of flight

Author contributions:
Guarantors of integrity of entire study, Y.Q., B.A.W.; study concepts/study design or data acquisition or data analysis/interpretation, all authors; manuscript drafting or manuscript revision for important intellectual content, all authors; approval of final version of submitted manuscript, all authors; literature research, Y.Q., S.R.Z., B.A.W.; clinical studies, all authors; statistical analysis, Y.Q., B.A.W.; and manuscript editing, all authors

Funding:
This research was supported by the National Institutes of Health (grant K99HL106232).

Conflicts of interest are listed at the end of this article.

assigned to *(a)* the acute group if they underwent imaging within 4 weeks after presentation, *(b)* the subacute group if they underwent imaging 4–12 weeks after presentation, or *(c)* the chronic group if they underwent imaging more than 12 weeks after presentation.

MR Imaging Examination

All examinations were performed with a 3-T MR imager (Achieva; Philips Healthcare, Best, the Netherlands) by using a body coil for transmission and an eight-channel head coil for reception. A standard MR imaging protocol was used that included pre- and postcontrast 3D BB MR imaging and 3D time-of-flight (TOF) MR angiographic sequences. The 3D TOF MR angiograms were acquired in a transverse plane by using the following parameters: repetition time msec/echo time msec, 23/3.5; flip angle, 25°; field of view, 160 ×160 mm; acquired resolution, 0.55 × 0.55 × 1.1 mm; and reconstructed resolution, 0.55 × 0.55 × 0.55 mm. Imaging time was approximately 6 minutes.

The 3D BB MR imaging sequence was then performed by using a volumetric isotropic turbo spin-echo acquisition (VISTA; Philips Healthcare, Best, the Netherlands) in a coronal plane (40-mm-thick slab) optimized for flow suppression and intracranial vessel wall delineation. Details of this sequence were published previously (12). A patent application was submitted by two authors (Y.Q., B.A.W.) for the BB MR imaging sequence described herein after this study was completed. The following parameters were used: 2000/38; turbo spin-echo factor, 56 echoes; echo spacing, 6.1 msec; sensitivity encoding factor, two; number of signals acquired, one; field of view, 180 × 180 × 40 mm; matrix, 450 × 450 × 100; acquired resolution, 0.4 × 0.4 × 0.4 mm; examination time, 7.2 minutes. A variable flip angle refocusing scheme was used with a minimum flip angle of 50° and a maximum flip angle of 120°, enabling high signal-to-noise efficiency and strong BB effects. Radial k-space view ordering was used to optimize T1-weighted contrast (17).

Gadopentetate dimeglumine (Magnevist; Schering, Berlin, Germany) was administered intravenously (0.1 mmol per kilogram of body weight), and BB MR imaging was repeated 5 minutes after contrast material administration.

Image Analysis

Plaque identification.—All MR images (MR angiograms and BB MR images) were interpreted by an independent neuroradiologist (B.A.W., 17 years of experience) for the presence of atherosclerotic lesions by using a picture archiving and communication system workstation (Ultravisual; Emageon, Birmingham, Ala). We used our picture archiving and communication system software to coregister and reconstruct the pre- and postcontrast 3D BB MR images and 3D TOF MR angiographic images in both short and long axes relative to the flow direction at the site of apparent wall thickening identified on the coronal source BB MR images. Atherosclerotic plaque on MR images was defined as eccentric wall thickening with or without luminal stenosis identified on both the reconstructed precontrast and the reconstructed postcontrast BB MR images. We were careful not to use the original source images for plaque identification (Fig 1, *B* and *C*) because the coronal imaging plane may not have optimally captured the vessel axis and because the vessel wall may have been only partially contained in each section. Lumen patency was assessed on the BB MR images at the site of apparent wall thickening and then compared with the corresponding location on the TOF MR angiogram. If narrowing was identified on the BB MR images but not on the TOF MR angiograms, the plaque was considered artifactual and was not counted. All plaques (ie, not only the plaque that qualified the patient for inclusion) were analyzed, regardless of the degree of stenosis. Because of the small size of intracranial vessels, we mainly focused on plaques involving the larger more proximal intracranial arteries, including M1 and M2 segments of the middle cerebral artery, A1 and A2 segments of the anterior cerebral artery, cavernous (C3) and supraclinoid (C4) segments of the internal carotid artery, P1 and P2 segments of the posterior cerebral artery, the basilar artery, and V4 segments of the vertebral arteries. All detectable plaques were recorded for each vessel segment.

Plaque contrast enhancement and thickness measurements.—Two independent readers (Y.Q., S.M.; 7 and 2 years of experience in plaque imaging, respectively) qualitatively graded plaque contrast enhancement based on its signal intensity on postcontrast BB MR images by using the corresponding precontrast series for reference. Readers were blinded to the characteristics of the study population, including brain MR imaging findings and clinical presentations. Plaque enhancement was graded by using a previously established grading scheme (18), as follows: grade 0 indicated enhancement was similar to or less than that of intracranial arterial walls without plaque in the same individual (Fig 1); grade 1, enhancement was greater than that of grade 0 but less than that of the pituitary infundibulum (Fig 2); and grade 2, enhancement was similar to or greater than that of the infundibulum (Fig 3). Cases in which readers disagreed were reviewed together and resolved by consensus.

MR images were then processed for all identified plaques by using commercially available software (VesselMass; Leiden University Medical Center, Leiden, the Netherlands). The 3D pre- and postcontrast BB MR images were reconstructed orthogonal to the vessel axis at 2.0-mm-thick sections through each plaque. Edge-enhanced (gradient) images were generated from the original grayscale images by using a Sobel operator (19) to eliminate the influence of subjective window and level settings for vessel contour detection. Lumen and outer wall contours were drawn on the reconstructed gradient images by using a semiautomated contouring feature of the aforementioned software. Plaque thickness (mean and maximum wall thickness) and signal intensity values were generated for the pre- and postcontrast series.

Plaque contrast enhancement was quantified by using the following equation: $CE = (S_{postBBMR} - S_{preBBMR})/S_{preBBMR}$ 3100, where CE is the percentage of contrast enhancement, $S_{postBBMR}$ is the

Figure 1

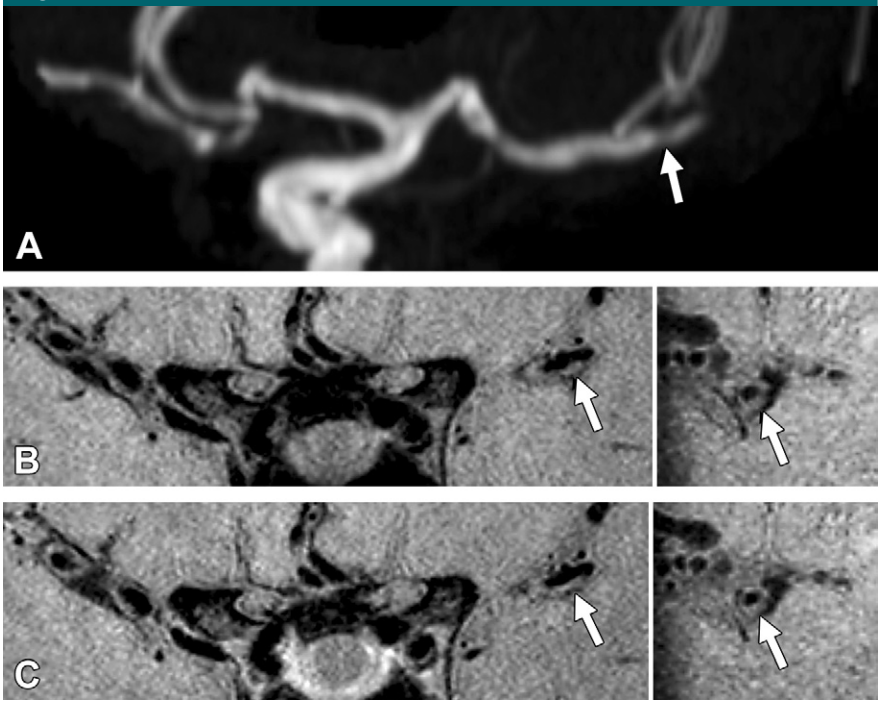

Figure 1: Grade 0 enhancement of a nonculprit plaque. *A*, TOF maximum intensity projection MR angiogram of the left middle cerebral artery shows moderate stenosis in the M2 segment (arrow) in a 61-year-old woman. *B*, Pre- and *C*, postcontrast 3D BB MR images (left: coronal acquisition) show wall thickening at the corresponding location (arrow). Right: Reconstructions perpendicular to flow direction through the wall thickening show an eccentric atherosclerotic plaque (arrow) with little to no enhancement, similar to that of normal intracranial arterial walls seen elsewhere in this patient.

normalized signal intensity on postcontrast BB MR images, and S_{preBBMR} is the normalized signal intensity on precontrast BB MR images. Plaque intensity was normalized to the signal intensity of adjacent brain parenchyma by using a manually placed measurement of a standard size (area, 15 mm^2), as reported previously (12).

Plaque classification.—Four neurologists (S.R.Z., R.L., V.U., and R.W.; 6.5, 7.5, 13, and 20 years of experience, respectively) independently classified each detected plaque according to its likelihood of causing the stroke by using a three-point confidence scale (0, nonculprit; 1, probably culprit; 2, culprit). The neurologists were provided each patient's clinical history and prior brain MR imaging studies obtained with diffusion-weighted and fluid-attenuated inversion recovery sequences and asked to determine the location of the recent stroke. They were also provided plaque locations, as determined by the neuroradiologist, based on review of the BB MR and MR angiographic images. The neurologists were not allowed to view the BB MR images directly, so degree of enhancement could not influence their decision. However, they were allowed to review recent angiographic studies (CT, MR, and/or conventional angiography) to help classify the likelihood that a plaque might have caused a stroke when multiple plaques were present in the same vascular territory.

The culprit plaque was identified based on the clinical presentation of the patient and clinical judgment of the neurologist. A plaque was considered a culprit plaque when it was *(a)* the only lesion within the vascular territory of the stroke or *(b)* the most stenotic lesion when multiple plaques were present within the same vascular territory of the stroke. A plaque was considered probably a culprit plaque when it was not the most stenotic lesion within the same vascular territory of the stroke. A lesion was considered a nonculprit plaque when it was not within the vascular territory of the stroke. For cases of transient ischemic attack, plaque classification was adjudicated if symptoms could be localized to an arterial territory. All disagreements were resolved by consensus.

Infarct characterization.—The locations and maximum diameters for all infarcts were recorded. Infarcts that were smaller than 2 cm in diameter and exclusively subcortical in location were defined as lacunae (20,21) and were excluded from our analysis since they are thought to have resulted from occlusion of small penetrating branches of large cerebral arteries (21).

Statistical Analysis

Data were analyzed by using Stata software (version 11.2; Stata, College Station, Tex). Categorical variables were presented as frequencies, and continuous variables were presented as means ± standard deviations. Multiple ordinal logistic regression analysis was used to estimate the association (odds ratio) of the likelihood of being a culprit lesion with both *(a)* plaque contrast enhancement (qualitative grade) and *(b)* plaque thickness (mean and maximum wall thickness). The dependent variables were categorized into three levels (culprit, probably culprit, and nonculprit) for this analysis. Robust variance estimates were used to account for repeated measurements within patients. Quantitative measurements of plaque contrast enhancement were compared between culprit, probably culprit, and nonculprit plaques by using the Kruskal-Wallis test and posthoc pairwise comparisons (Wilcoxon rank sum tests). Interreader agreement for plaque enhancement and plaque classifications were estimated based on all detected lesions by using κ coefficients before reader consensus to settle disagreements. Reliabilities less than 0.4 were characterized as poor, reliabilities of 0.4–0.75 were characterized as fair to good, and reliabilities greater than 0.75 were considered excellent

Figure 2

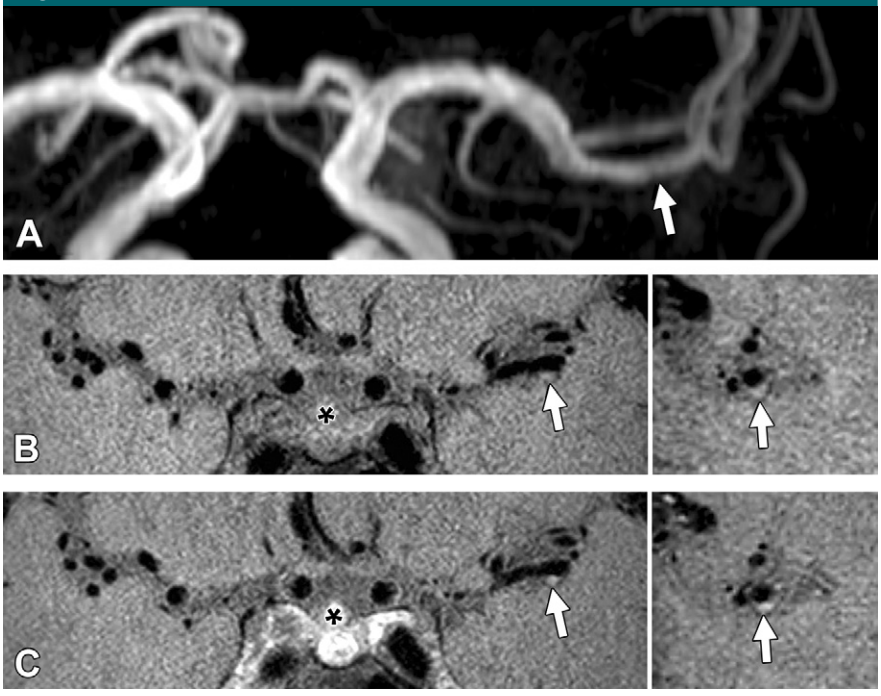

Figure 2: Grade 1 enhancement of a probably culprit plaque. *A*, TOF maximum intensity projection MR angiogram of the left middle cerebral artery shows mild stenosis in the M1 segment (arrow) in a 42-year-old man with a nearly occlusive basilar plaque. *B*, Pre- and, *C*, postcontrast 3D BB MR images (left: coronal acquisition) show wall thickening at the corresponding location (arrow). Right: Reconstructions perpendicular to flow direction through the wall thickening show an eccentric atherosclerotic plaque (arrow) with enhancement greater than that of normal intracranial arteries elsewhere but less than that of the pituitary infundibulum (*).

(22). A *P* value less than .05 was considered indicative of a significant difference.

Results

Patient Characteristics

Among the 27 patients (19 male; 15 white, 10 African American, one Asian, one Hispanic; mean age, 56.8 years ± 12.4), 25 had ischemic strokes (acute stroke, *n* = 20; subacute stroke, *n* = 2; chronic stroke, *n* = 3) and two had transient ischemic attacks. Only one lacunar infarct (8.8 mm, right basal ganglia) was identified, and it was categorized as chronic. The median interval between symptom onset and BB MR imaging was 21 days (interquartile range, 4 days to 4 months). A total of 99 plaques were identified in the 27 patients, with multiple plaques seen in 24 (89%). The clinical characteristics of the study population are shown in Table 1 and Table E1 (online).

Seventy-eight plaques were identified in the 20 patients with acute stroke, with multiple plaques seen in 17 (85%) (mean, 3.5 plaques per patient; range, one to 14 plaques) (Table 1). Fifty plaques were detected in the anterior circulation (anterior cerebral artery, *n* = 7; internal carotid artery, *n* = 26; and middle cerebral artery, *n* = 17), and 28 were detected in the posterior circulation (basilar artery, *n* = 13; posterior cerebral artery, *n* = 6; and vertebral artery, *n* = 9). Twenty-one (27%) plaques were deemed culprit plaques (anterior circulation, *n* = 11; posterior circulation, *n* = 10), 12 (15%) were deemed probably culprit plaques (anterior, *n* = 9; posterior circulation, *n* = 3), and 45 (58%) were deemed nonculprit plaques (anterior, *n* = 30; posterior circulation, *n* = 15).

Plaque Enhancement after Contrast Agent Administration

Among the 78 plaques identified in patients with acute stroke, 64 (82%) enhanced (ie, grade 1 or 2). All 21 culprit plaques enhanced (grade 1, 10%; grade 2, 90%), all 12 probably culprit plaques enhanced (grade 1, 67%; grade 2, 33%), and 31 (69%) of 45 nonculprit plaques enhanced (grade 1, 47%; grade 2, 22%) (Table 2). A culprit plaque with its downstream infarction is shown in Figure 4. Grade 0 was observed in only nonculprit plaques.

Culprit plaques were associated with a higher grade of plaque enhancement (odds ratio, 5.5; 95% confidence interval [CI]: 2.4, 12.5) and with greater plaque thickness (mean wall thickness: odds ratio, 2.6; 95% confidence interval: 1.2, 5.5) (maximum wall thickeness: odds ratio, 1.7; 95% confidence interval: 1.1, 2.5) based on univariate logistic regression models. Grade 2 enhancement was independently associated with culprit plaques (compared with grade 0: odds ratio, 34.6; 95% CI: 4.5, 266.5; *P* = .001), whereas grade 1 was not (compared with grade 0: odds ratio, 4.8; 95% CI: 0.5, 42.9; *P* = .16) when adjusted for plaque thickness (mean and maximum wall thickness). Neither mean wall thickness nor maximum wall thickness was associated with culprit plaques (*P* = .27 and *P* = .99, respectively).

Plaque degree of contrast enhancement quantified for all 78 plaques showed significant differences when grouped by lesion type (ie, nonculprit, probably culprit, and culprit) with a Kruskal-Wallis test ($P < .001$). In pairwise comparisons (Fig 5), the degree of contrast enhancement of nonculprit plaques (mean, 13.6% ± 12.3) was nearly half that of probably culprit plaques (mean, 25.8% ± 15.0; *P* = .02) and culprit plaques (mean, 25.9% ± 13.4; *P* = .003).

Plaque contrast enhancement persisted beyond the acute stage. Nine plaques were identified in the two patients with subacute stroke (culprit, *n* = 2; probably culprit, *n* = 4; nonculprit, *n* = 3), and all plaques showed contrast enhancement (grade 1, *n* = 5; grade 2, *n* = 4). Nine plaques were identified in the three

Figure 3

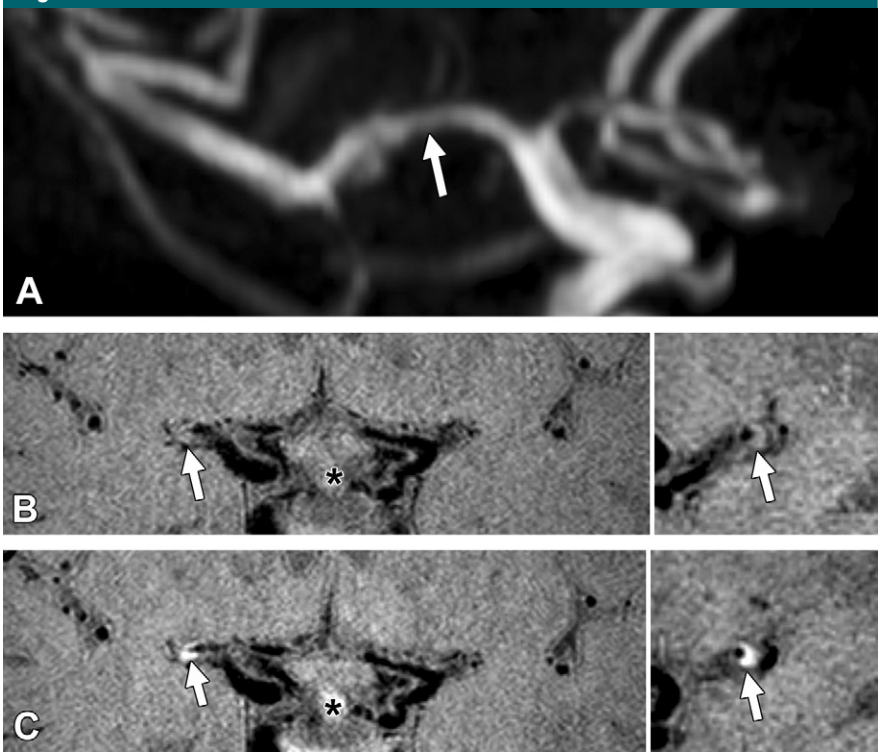

Figure 3: Grade 2 enhancement of a culprit plaque. *A*, TOF maximum intensity projection MR angiogram of the right middle cerebral artery shows mild to moderate stenosis of the M1 segment (arrow) in a 61-year-old woman. *B*, Pre- and, *C*, postcontrast 3D VISTA images (left: coronal acquisition) show wall thickening at the corresponding location (arrow). Right: Reconstructions perpendicular to flow direction through the wall thickening show an eccentric atherosclerotic plaque (arrow) with enhancement greater than that of the pituitary infundibulum (*).

Table 1

Demographic, Clinical, and Plaque Characteristics of Patients

Characteristic	No. of Patients
Patient characteristic*	
Male sex	19 (70)
Active smoker	4 (15)
Diabetes mellitus	9 (33)
Hypertension	22 (81)
Hyperlipidemia	16 (59)
Stroke	25 (93)
Acute	20 (74)
Subacute	2 (7)
Chronic	3 (11)
Transient ischemic attack	2 (7)
No. of plaques identified per patient†	
1	3 (15)
2	3 (15)
3	6 (30)
4	1 (5)
≥5	7 (35)
Plaque location†	
Anterior cerebral artery	7 (9)
Internal carotid artery	26 (33)
Middle cerebral artery	17 (22)
Basilar artery	13 (17)
Posterior cerebral artery	6 (8)
Vertebral artery	9 (12)
Plaque classification†	
Nonculprit	45 (58)
Probably culprit	12 (15)
Culprit	21 (27)

Note.—Data in parentheses are percentages.

* For the entire cohort of 27 patients.

† For the 20 patients with an acute stroke (78 plaques).

patients with chronic stroke (culprit, n = 1; probably culprit, n = 4; and nonculprit, n = 4), and eight (89%) plaques demonstrated contrast enhancement (grade 1, n = 1; grade 2, n = 7). The interval between stroke onset and MR imaging in patients with chronic stroke ranged from 5 months to 1.5 years.

MR Imaging Measurement Reproducibility

Interreader agreement for determining lesion type (culprit, probably culprit, or nonculprit) was excellent (weighted κ = 0.83; 95% CI: 0.72, 0.93). Interreader agreement for grading plaque enhancement was excellent (weighted κ = 0.81; 95% CI: 0.71, 0.92).

Discussion

We have shown that contrast enhancement of an intracranial atherosclerotic plaque is associated with its likelihood to have caused a recent ischemic event, and this is independent of its thickness. Our findings extend those of previous reports that extracranial plaque enhancement is associated with inflammation and plaque disruption (7,8). This feature might serve as a marker of intracranial plaque instability, providing insight into stroke risk and highlighting the importance of 3D contrast-enhanced MR imaging in ICAD evaluation.

To our knowledge, this is the first in vivo study to distinguish features of culprit plaques from those of stable intracranial plaques with 3D high-spatial-resolution BB MR imaging, thereby providing an internal control for environmental and genetic variations. In comparison with standard two-dimensional BB MR imaging techniques (13,23), a 3D acquisition offers a considerable advantage for imaging intracranial vessels because of its broad coverage, enabling a comprehensive survey of intracranial plaques at typical sites of involvement (12). In addition, the inherent ability to reconstruct 3D isotropic volume acquisitions in any plane enables retrospective visualization of plaques involving tortuous vessels, which is particularly helpful when analyzing the innately curved intracranial arteries. Furthermore, our acquired resolution (0.4 mm^3) is the highest reported for in vivo vessel wall imaging, thus facilitating the depiction of intracranial plaques given the small size of these vessels.

Table 2

Enhancement Grade of Nonculprit, Probably Culprit, and Culprit Plaques in Patients with Acute Stroke

Plaque	Enhancement Grade 0	Enhancement Grade 1	Enhancement Grade 2	Total
Nonculprit	14	21	10	45
Probably culprit	0	8	4	12
Culprit	0	2	19	21

Figure 4

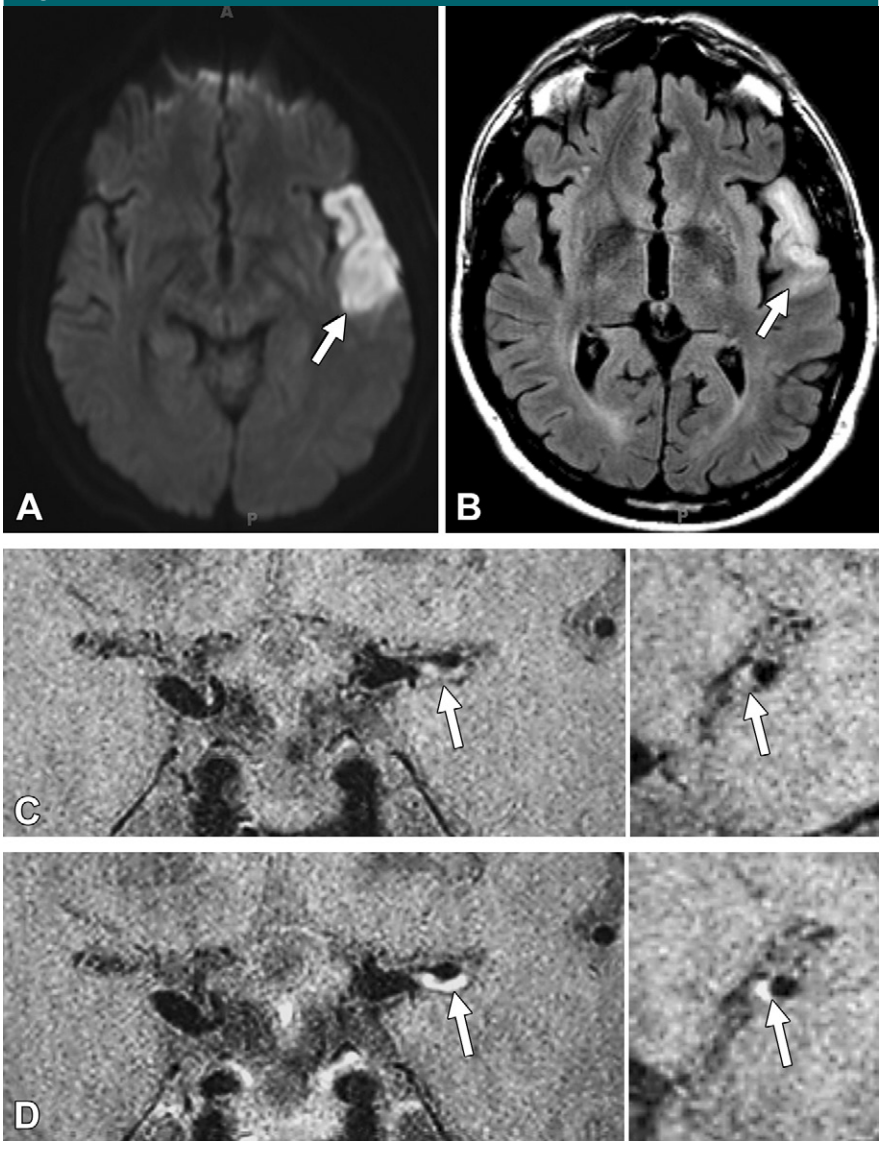

Figure 4: Acute infarction downstream from a culprit plaque with grade 2 enhancement in a 40-year-old man. *A*, Diffusion-weighted MR image shows restricted diffusion (arrow) in left temporal lobe. *B*, Fluid attenuated inversion-recovery MR image shows corresponding hyperintense signal intensity (arrow). *C*, Pre- and, *D*, post-contrast 3D BB MR images (left: coronal acquisition) show eccentric wall thickening, with grade 2 enhancement of left M1 segment (arrow). Right: Reconstructions perpendicular to flow direction through wall thickening show eccentric atherosclerotic plaque (arrows).

Our findings that ICAD lesions often involve multiple intracranial vascular beds (15,24) and that inflammation might play a key role in the occurrence of ischemic stroke (3) are consistent with pathologic observations in autopsy specimens.

Contrast enhancement has been recognized as an important marker of plaque vulnerability in extracranial carotid and coronary arteries (7,8,11). In the carotid artery territory, selective contrast enhancement seen on MR images occurs preferentially in the fibrous cap, corresponding to histologic markers of inflammation, including staining for macrophage presence and neovascularization (25,26). Furthermore, there is strong evidence that carotid plaque enhancement is a marker of inflammation (8) and relates to cerebrovascular ischemic events (7,27). In fact, degree of plaque enhancement has been shown to relate to stroke risk when stenosis does not in some groups with carotid plaque (7,28). In the coronary artery, MR imaging has shown wall enhancement in patients with acute myocardical infarction; this enhancement is associated with elevated systemic inflammatory markers (11,24). Strong contrast enhancement is thought to relate to greater neovascularization and increased endothelial permeability, both of which facilitate the delivery and accumulation of the contrast agent into plaque (8,29–32) and predispose the patient to future plaque disruption (33). Our results extend these observations in extracranial vessels by suggesting that the high degree of enhancement seen in patients with intracranial plaques responsible for ischemic events likely reflects increased inflammatory activity. As with extracranial plaque enhancement, enhancement identified in patients with intracranial plaques might serve as a more precise marker of stroke risk than would measuring stenosis, potentially enabling risk stratification in low-grade or even angiographically occult lesions (11,27).

In this study, plaque enhancement was evaluated both qualitatively and quantitatively. The qualitative grading scheme is easily implemented in clinical practice and offers immediate insight

Figure 5

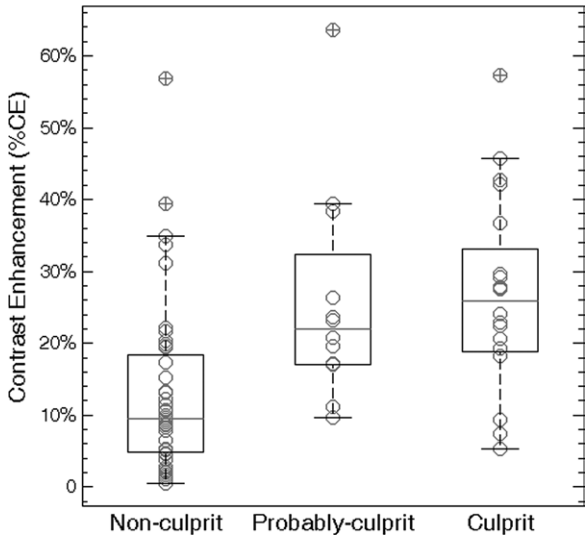

Figure 5: Graph comparing degree of contrast enhancement for nonculprit, probably culprit and culprit plaques. Box-and-whisker plots represent medians (lines within boxes), interquartile ranges (upper and lower ends of boxes), greatest and least values (top and bottom lines), and outliers (data points beyond top and bottom lines) for degree of contrast enhancement. Circles represent individual data points. Nonculprit plaques had a lower degree of contrast enhancement than did probably culprit (13.6% ± 12.3 vs 25.8% ± 15.0, $P = .02$) and culprit (13.6% ± 12.3 vs 25.9% ± 13.4, $P = .003$) plaques. However, there was no difference in degree of contrast enhancement between probably culprit and culprit plaques ($P = .71$).

into plaque risk. The quantitative analysis minimizes operator dependence and further validates our qualitative results.

Interestingly, we found that some nonculprit plaques (ie, lowest likelihood to cause a stroke) demonstrated some enhancement, although to a lesser degree. This finding was not observed in a small case series previously reported (34) in which four asymptomatic plaques in eight patients were identified without evidence of enhancement; however, this difference could be explained by sample size differences (ie, 45 nonculprit plaques in our study). Furthermore, since no definition of enhancement was given in this prior report, their results cannot be compared with our results without knowing their reference standard. Although we identified contrast enhancement in culprit and nonculprit plaques, we observed a lack of enhancement only in nonculprit plaques (Table 2). This suggests that this technique might be better suited to identification of stable rather than unstable lesions. This could have direct clinical applications, since a lack of enhancement might direct against more aggressive management strategies, thereby averting the high risk of such procedures (35–37). However, validation with prospective studies would be needed before this imaging feature could be considered for clinical implementation.

There were several limitations to our study. First, a prospective study is needed to validate plaque enhancement as a predictor of future events. Second, although gadolinium contrast enhancement is well established in the identification of sites of inflammation, including those within extracranial plaque (7,8,38), the exact mechanism accounting for intracranial plaque enhancement remains unknown due to the lack of available histologic correlation. Further studies in which researchers used molecular contrast agents to target specific inflammatory features (39,40) of intracranial plaques, such as macrophage-targeted iron oxide nanoparticles (41), could help to clarify the basis of enhancement. Third, current MR imaging techniques are incapable of reliably characterizing individual ICAD plaque components (eg, fibrous cap, lipid core, and intraplaque hemorrhage); thus, a global measure of plaque enhancement was used rather than enhancement of specific components. Fourth, our 3D BB MR image acquisition was not purely T1 weighted, since there was mixed proton density–weighted contrast. Like T1-weighted imaging, proton density–weighted imaging is capable of depicting plaque enhancement (25); however, its inherently higher achievable signal is preferable, given the high signal needed to resolve the intracranial vessel wall. Fifth, our study population consisted of patients with ICAD causing intracranial arterial stenosis of 50% or more. Further prospective studies that include participants with low-grade stenosis would contribute to a more comprehensive understanding of stroke risk.

In conclusion, we have shown that intracranial atherosclerotic plaque enhancement can be used to identify lesions responsible for cerebrovascular ischemic events. This feature may serve as a marker of intracranial plaque vulnerability and provide insight into risk for future events, enabling the identification of individuals who harbor an occult burden of vulnerable features and who might benefit from preventive therapeutic interventions.

Disclosures of Conflicts of Interest: Y.Q. Financial activities related to the present article: none to disclose. Financial activities not related to the present article: has a patent pending (no. 13/922,111) for the MR imaging technique used in this study. Other relationships: none to disclose. **S.R.Z.** No potential conflicts of interest to disclose. **S.M.** No potential conflicts of interest to disclose. **R.L.** No potential conflicts of interest to disclose. **V.U.** No potential conflicts of interest to disclose. **R.W.** No potential conflicts of interest to disclose. **B.A.W.** Financial activities related to the present article: none to disclose. Financial activities not related to the present article: has a patent pending (no. 13/922,111) for the MR imaging technique used in this study. Other relationships: none to disclose.

References

1. Wityk RJ, Lehman D, Klag M, Coresh J, Ahn H, Litt B. Race and sex differences in the distribution of cerebral atherosclerosis. Stroke 1996;27(11):1974–1980.
2. Wong LK. Global burden of intracranial atherosclerosis. Int J Stroke 2006;1(3):158–159.
3. Chen XY, Wong KS, Lam WW, Zhao HL, Ng HK. Middle cerebral artery atherosclerosis: histological comparison between plaques associated with and not associated with infarct in a postmortem study. Cerebrovasc Dis 2008;25(1-2):74–80.
4. Mazighi M, Labreuche J, Gongora-Rivera F, Duyckaerts C, Hauw JJ, Amarenco P. Au-

topsy prevalence of intracranial atherosclerosis in patients with fatal stroke. Stroke 2008; 39(4):1142–1147.

5. Labadzhyan A, Csiba L, Narula N, Zhou J, Narula J, Fisher M. Histopathologic evaluation of basilar artery atherosclerosis. J Neurol Sci 2011;307(1-2):97–99.
6. Arenillas JF, Alvarez-Sabín J, Molina CA, et al. Progression of symptomatic intracranial large artery atherosclerosis is associated with a proinflammatory state and impaired fibrinolysis. Stroke 2008;39(5):1456–1463.
7. Qiao Y, Etesami M, Astor BC, Zeiler SR, Trout HH 3rd, Wasserman BA. Carotid plaque neovascularization and hemorrhage detected by MR imaging are associated with recent cerebrovascular ischemic events. AJNR Am J Neuroradiol 2012;33(4):755–760.
8. Kerwin WS, Oikawa M, Yuan C, Jarvik GP, Hatsukami TS. MR imaging of adventitial vasa vasorum in carotid atherosclerosis. Magn Reson Med 2008;59(3):507–514.
9. Aoki S, Shirouzu I, Sasaki Y, et al. Enhancement of the intracranial arterial wall at MR imaging: relationship to cerebral atherosclerosis. Radiology 1995;194(2):477–481.
10. Rudd JH, Fayad ZA. Imaging atherosclerotic plaque inflammation. Nat Clin Pract Cardiovasc Med 2008;5(Suppl 2):S11–S17.
11. Ibrahim T, Makowski MR, Jankauskas A, et al. Serial contrast-enhanced cardiac magnetic resonance imaging demonstrates regression of hyperenhancement within the coronary artery wall in patients after acute myocardial infarction. JACC Cardiovasc Imaging 2009;2(5):580–588.
12. Qiao Y, Steinman DA, Qin Q, et al. Intracranial arterial wall imaging using three-dimensional high isotropic resolution black blood MRI at 3.0 Tesla. J Magn Reson Imaging 2011;34(1):22–30.
13. Swartz RH, Bhuta SS, Farb RI, et al. Intracranial arterial wall imaging using high-resolution 3-tesla contrast-enhanced MRI. Neurology 2009;72(7):627–634.
14. Antiga L, Wasserman BA, Steinman DA. On the overestimation of early wall thickening at the carotid bulb by black blood MRI, with implications for coronary and vulnerable plaque imaging. Magn Reson Med 2008;60(5): 1020–1028.
15. Nahab F, Cotsonis G, Lynn M, et al. Prevalence and prognosis of coexistent asymptomatic intracranial stenosis. Stroke 2008; 39(3):1039–1041.
16. Chimowitz MI, Kokkinos J, Strong J, et al. The Warfarin-Aspirin Symptomatic Intracranial Disease Study. Neurology 1995;45(8):1488–1493.
17. Busse RF, Brau AC, Vu A, et al. Effects of refocusing flip angle modulation and view ordering in 3D fast spin echo. Magn Reson Med 2008;60(3):640–649.
18. van der Kolk AG, Zwanenburg JJ, Brundel M, et al. Intracranial vessel wall imaging at 7.0-T MRI. Stroke 2011;42(9):2478–2484.
19. Greenman RL, Wang X, Ngo L, Marquis RP, Farrar N. An assessment of the sharpness of carotid artery tissue boundaries with acquisition voxel size and field strength. Magn Reson Imaging 2008;26(2):246–253.
20. Longstreth WT Jr, Bernick C, Manolio TA, Bryan N, Jungreis CA, Price TR. Lacunar infarcts defined by magnetic resonance imaging of 3660 elderly people: the Cardiovascular Health Study. Arch Neurol 1998; 55(9):1217–1225.
21. Fisher CM. Lacunar strokes and infarcts: a review. Neurology 1982;32(8):871–876.
22. Fleiss J. Statistical methods for rates and proportions. 2nd ed. New York, NY: Wiley, 1981; 218.
23. Xu WH, Li ML, Gao S, et al. In vivo high-resolution MR imaging of symptomatic and asymptomatic middle cerebral artery atherosclerotic stenosis. Atherosclerosis 2010; 212(2):507–511.
24. Kern R, Steinke W, Daffertshofer M, Prager R, Hennerici M. Stroke recurrences in patients with symptomatic vs asymptomatic middle cerebral artery disease. Neurology 2005;65(6):859–864.
25. Wasserman BA, Smith WI, Trout HH 3rd, Cannon RO 3rd, Balaban RS, Arai AE. Carotid artery atherosclerosis: in vivo morphologic characterization with gadolinium-enhanced double-oblique MR imaging initial results. Radiology 2002;223(2):566–573.
26. Yuan C, Kerwin WS, Ferguson MS, et al. Contrast-enhanced high resolution MRI for atherosclerotic carotid artery tissue characterization. J Magn Reson Imaging 2002;15(1): 62–67.
27. Wasserman BA. Advanced contrast-enhanced MRI for looking beyond the lumen to predict stroke: building a risk profile for carotid plaque. Stroke 2010;41(10 Suppl):S12–S16.
28. Wasserman BA, Wityk RJ, Trout HH 3rd, Virmani R. Low-grade carotid stenosis: looking beyond the lumen with MRI. Stroke 2005; 36(11):2504–2513.
29. de Boer OJ, van der Wal AC, Teeling P, Becker AE. Leucocyte recruitment in rupture prone regions of lipid-rich plaques: a prominent role for neovascularization? Cardiovasc Res 1999;41(2):443–449.
30. Celletti FL, Waugh JM, Amabile PG, Brendolan A, Hilfiker PR, Dake MD. Vascular endothelial growth factor enhances atherosclerotic plaque progression. Nat Med 2001;7(4): 425–429.
31. Rudd JH, Warburton EA, Fryer TD, et al. Imaging atherosclerotic plaque inflammation with [18F]-fluorodeoxyglucose positron emission tomography. Circulation 2002;105(23): 2708–2711.
32. Calcagno C, Cornily JC, Hyafil F, et al. Detection of neovessels in atherosclerotic plaques of rabbits using dynamic contrast enhanced MRI and 18F-FDG PET. Arterioscler Thromb Vasc Biol 2008;28(7):1311–1317.
33. Phinikaridou A, Ruberg FL, Hallock KJ, et al. In vivo detection of vulnerable atherosclerotic plaque by MRI in a rabbit model. Circ Cardiovasc Imaging 2010;3(3):323–332.
34. Vergouwen MD, Silver FL, Mandell DM, Mikulis DJ, Swartz RH. Eccentric narrowing and enhancement of symptomatic middle cerebral artery stenoses in patients with recent ischemic stroke. Arch Neurol 2011;68(3):338–342.
35. Lau AY, Zhao Y, Chen C, et al. Dual antiplatelets reduce microembolic signals in patients with transient ischemic attack and minor stroke: subgroup analysis of CLAIR study. Int J Stroke 2013 Mar 12. [Epub ahead of print]
36. Wang TH, Bhatt DL, Fox KA, et al. An analysis of mortality rates with dual-antiplatelet therapy in the primary prevention population of the CHARISMA trial. Eur Heart J 2007;28(18):2200–2207.
37. Chimowitz MI, Lynn MJ, Derdeyn CP, et al. Stenting versus aggressive medical therapy for intracranial arterial stenosis. N Engl J Med 2011;365(11):993–1003.
38. Aoki S, Aoki K, Ohsawa S, Nakajima H, Kumagai H, Araki T. Dynamic MR imaging of the carotid wall. J Magn Reson Imaging 1999; 9(3):420–427.
39. Lipinski MJ, Amirbekian V, Frias JC, et al. MRI to detect atherosclerosis with gadolinium-containing immunomicelles targeting the macrophage scavenger receptor. Magn Reson Med 2006;56(3):601–610.
40. Nahrendorf M, Jaffer FA, Kelly KA, et al. Noninvasive vascular cell adhesion molecule-1 imaging identifies inflammatory activation of cells in atherosclerosis. Circulation 2006; 114(14):1504–1511.
41. Kooi ME, Cappendijk VC, Cleutjens KB, et al. Accumulation of ultrasmall superparamagnetic particles of iron oxide in human atherosclerotic plaques can be detected by in vivo magnetic resonance imaging. Circulation 2003;107(19):2453–2458.